

## Supporting Information

# ZnO Nanoconfined 3D Porous Carbon Composite Microspheres to Stabilize Lithium Nucleation/Growth for High-Performance Lithium Metal Anodes

*Linsheng Tang,<sup>a</sup> Rui Zhang,<sup>a</sup> Xinyue Zhang,<sup>d</sup> Naiqin Zhao,<sup>abc</sup> Chunsheng Shi,<sup>a</sup> Enzuo Liu,<sup>a b</sup> Liying Ma,<sup>a</sup> Jiayan Luo \*<sup>d</sup> and Chunnnian He\*<sup>abc</sup>*

<sup>a</sup>School of Materials Science and Engineering and Tianjin Key Laboratory of Composites and Functional Materials, Tianjin University, Tianjin 300072, P. R. China.  
E-mail: cnhe08@tju.edu.cn

<sup>b</sup>Collaborative Innovation Center of Chemical Science and Engineering, Tianjin 300072, China

<sup>c</sup>Key Laboratory of Advanced Ceramics and Machining Technology, Ministry of Education, Tianjin University, Tianjin 300072, China

<sup>d</sup>Key Laboratory for Green Chemical Technology of Ministry of Education, School of Chemical Engineering and Technology, Tianjin University, Tianjin 300072, China. E-mail: jluo@tju.edu.cn

**Keywords:** Lithium metal anode, composite microsphere, nanoconfined structure, nucleation seed, 3D scaffolds

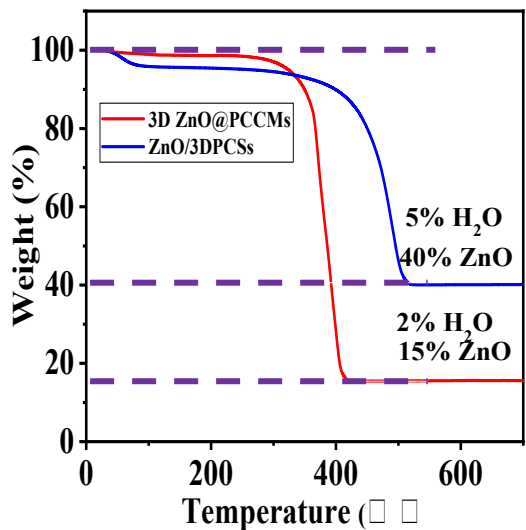


Fig. S1. TGA profiles of 3D ZnO@PCCMs and ZnO/3DPCSSs. On the basis of the final weight of ZnO, the original contents of ZnO in the 3D ZnO@PCCMs and ZnO/3DPCSSs were calculated to be ~15 wt.% and ~40 wt.%, respectively.

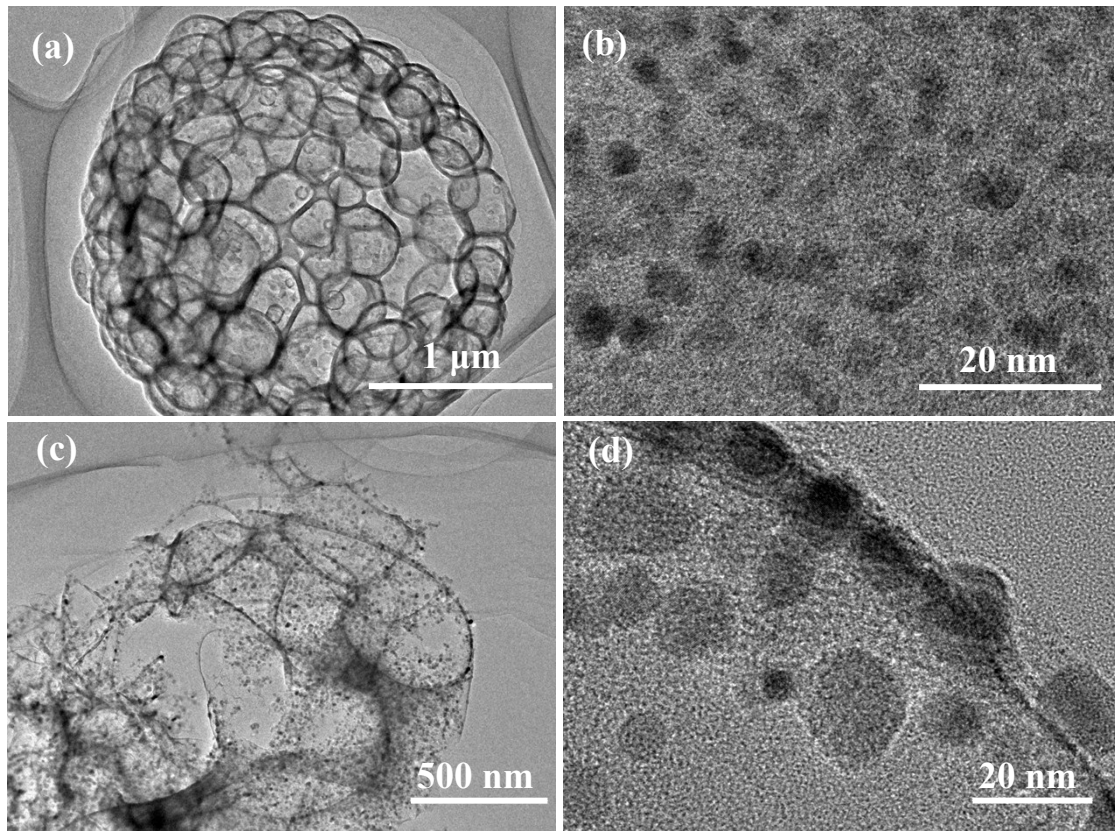


Fig. S2. TEM images of (a)(b) 3D ZnO@PCCMs, and (c)(d) ZnO/3DPCSs.

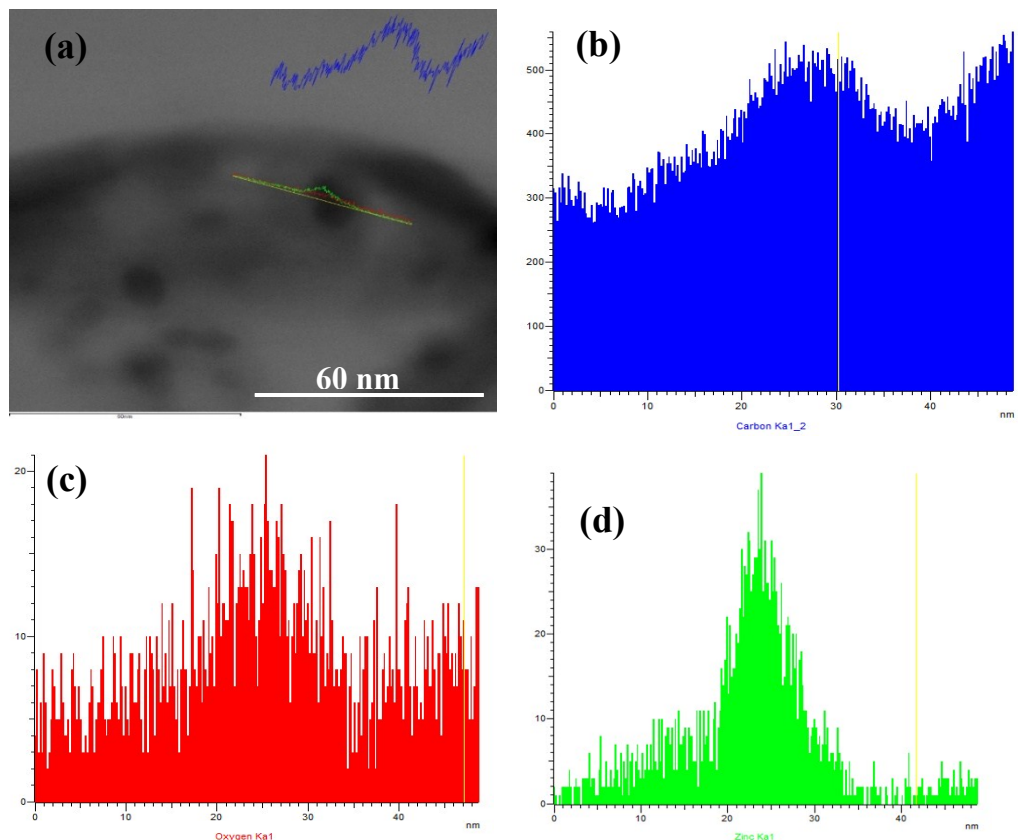


Fig. S3. (b) C, (c) O and (d) Zn cross-sectional EDX elemental mapping of point in (a).

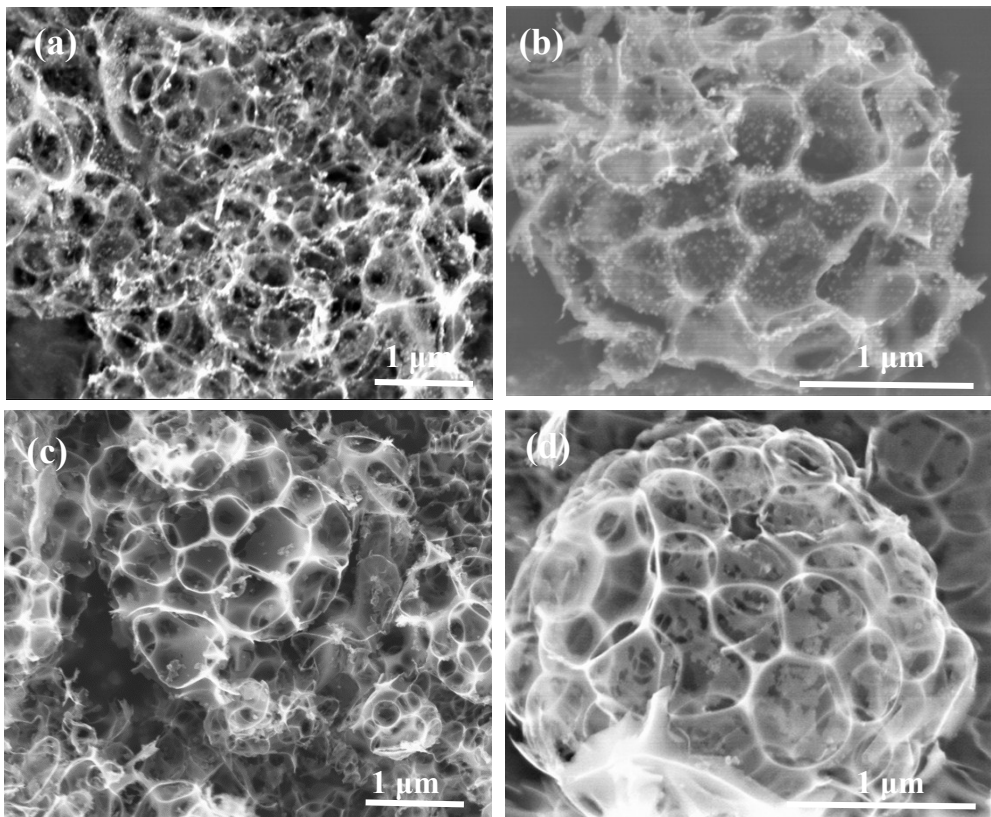


Fig. S4. SEM images of (a, b) ZnO/3DPCSs and (c, d) 3DPCSs with different magnification.

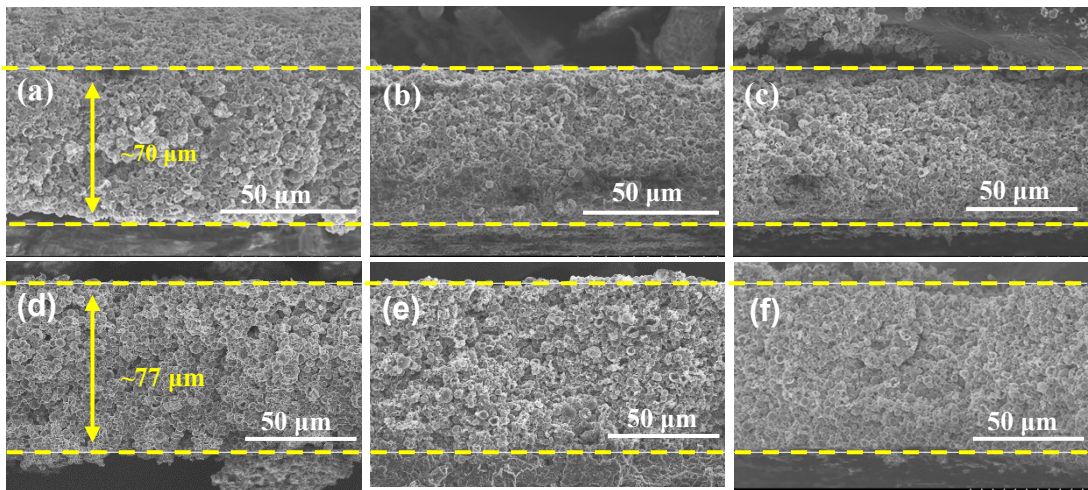


Fig. S5. Cross-sectional SEM images of (a) the pristine 3D ZnO@PCCMs electrode, after plating (b)  $0.1 \text{ mA h cm}^{-2}$  Li, (c)  $0.5 \text{ mA h cm}^{-2}$  Li, (d)  $2.0 \text{ mA h cm}^{-2}$  Li, (e)  $5.0 \text{ mA h cm}^{-2}$  Li and (f) after stripping  $5.0 \text{ mA h cm}^{-2}$  Li.

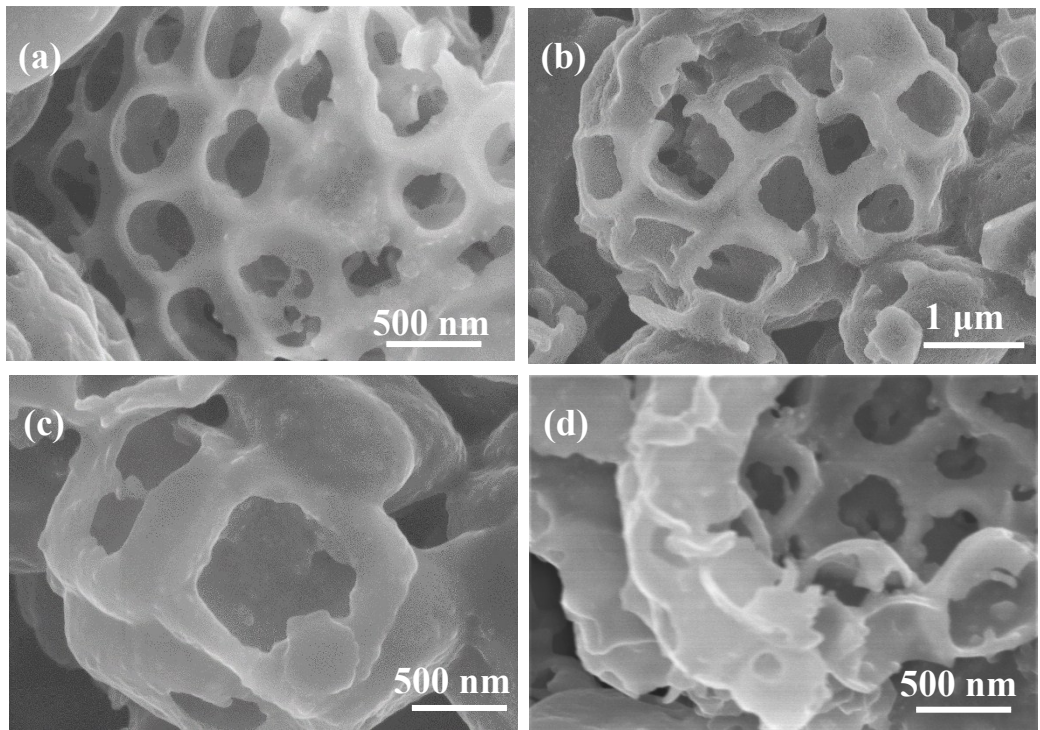


Fig. S6. Surface morphology of Li metal anodes. SEM images of 3D ZnO@PCCMs electrode after plating (a)  $0.5 \text{ mA h cm}^{-2}$ , (b)  $2.0 \text{ mA h cm}^{-2}$ , (c)  $5.0 \text{ mA h cm}^{-2}$  and (d) after stripping  $5.0 \text{ mA h cm}^{-2}$ .

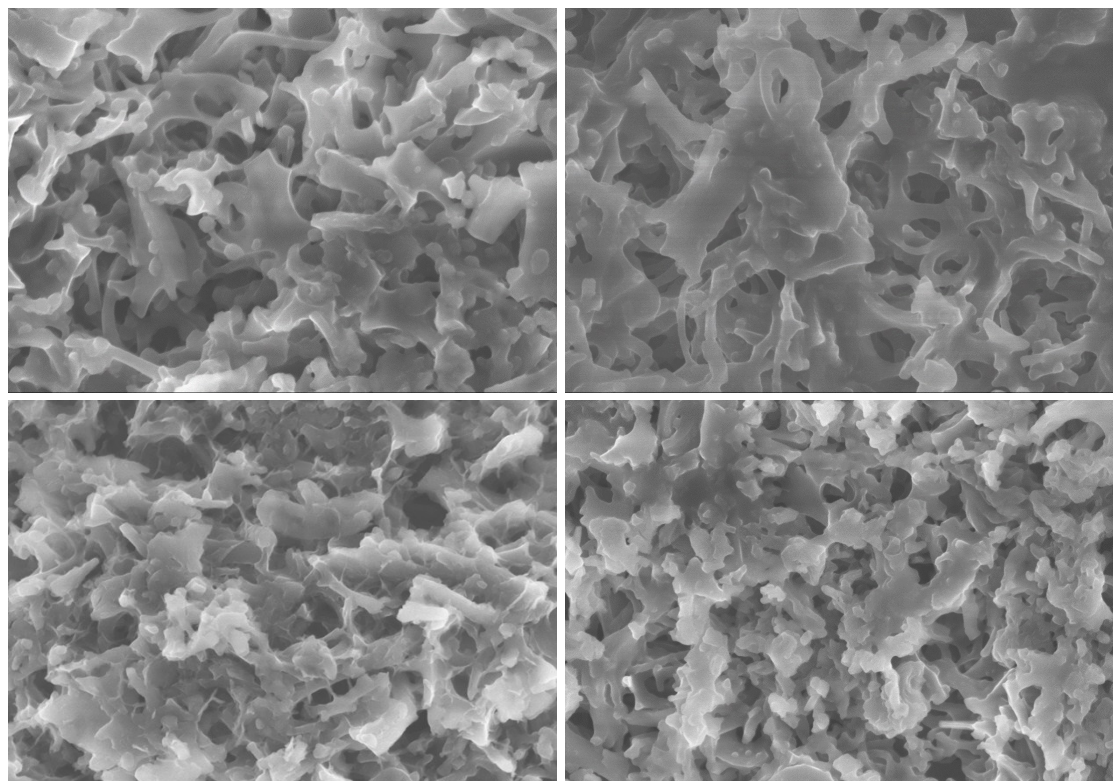


Fig. S7. SEM images of the 3DPCSS electrode after plating (a)  $0.5 \text{ mAh cm}^{-2}$  Li, (b)  $2.0 \text{ mAh cm}^{-2}$  Li, (c)  $5.0 \text{ mAh cm}^{-2}$  Li and (d) after stripping  $5.0 \text{ mA h cm}^{-2}$  Li.

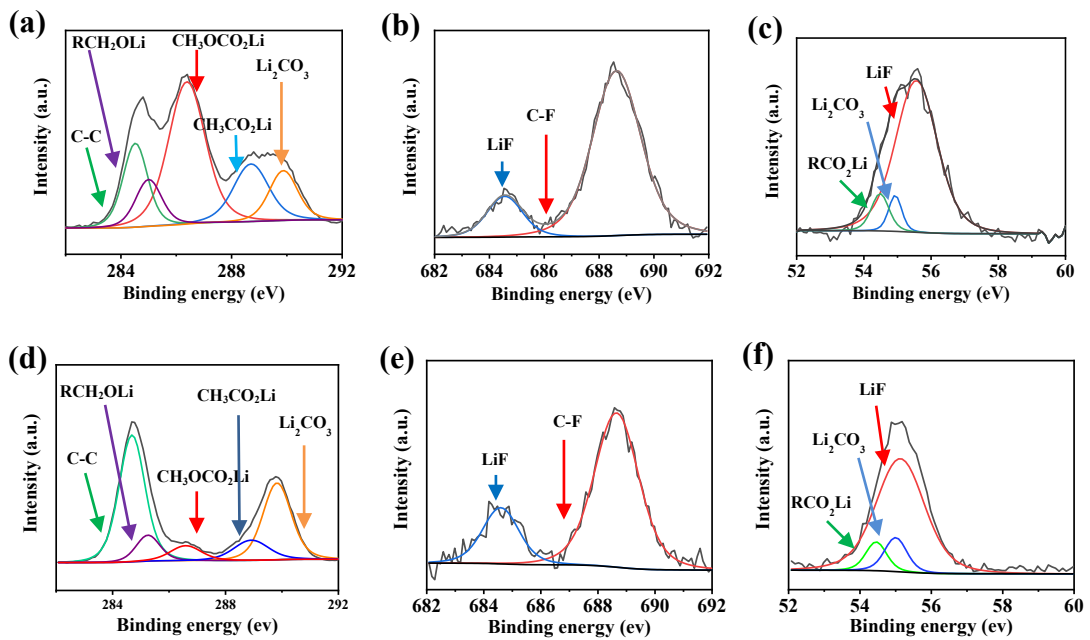


Fig. S8. Surface composition on the 3D ZnO@PCCMs electrode after Li stripping 1s and 50s. (a) and (d) C 1s, (b) and (e) F 1s, (c) and (f) Li 1s XPS spectra of SEI layer on the surface of the 3D ZnO@PCCMs electrode.

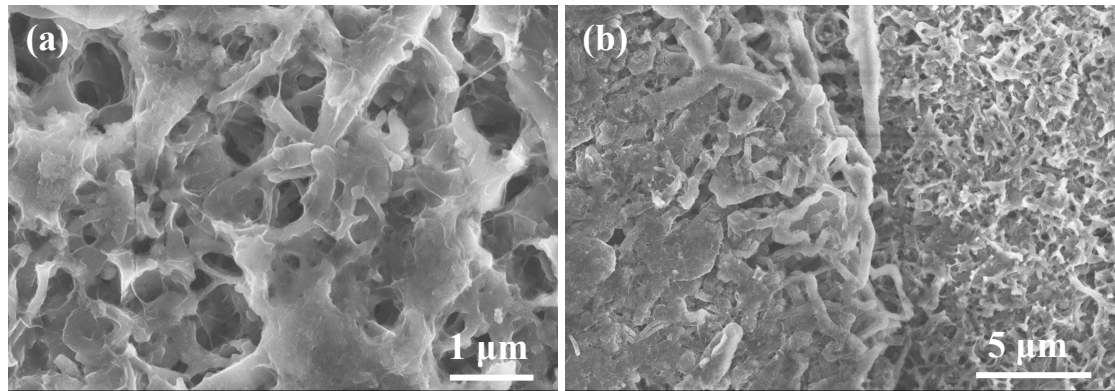


Fig. S9. SEM images of the 3DPCSs electrode with Li depositing at 1 mA/cm<sup>2</sup> for 2.0 mAh/cm<sup>2</sup> after 50 plating/stripping cycles.

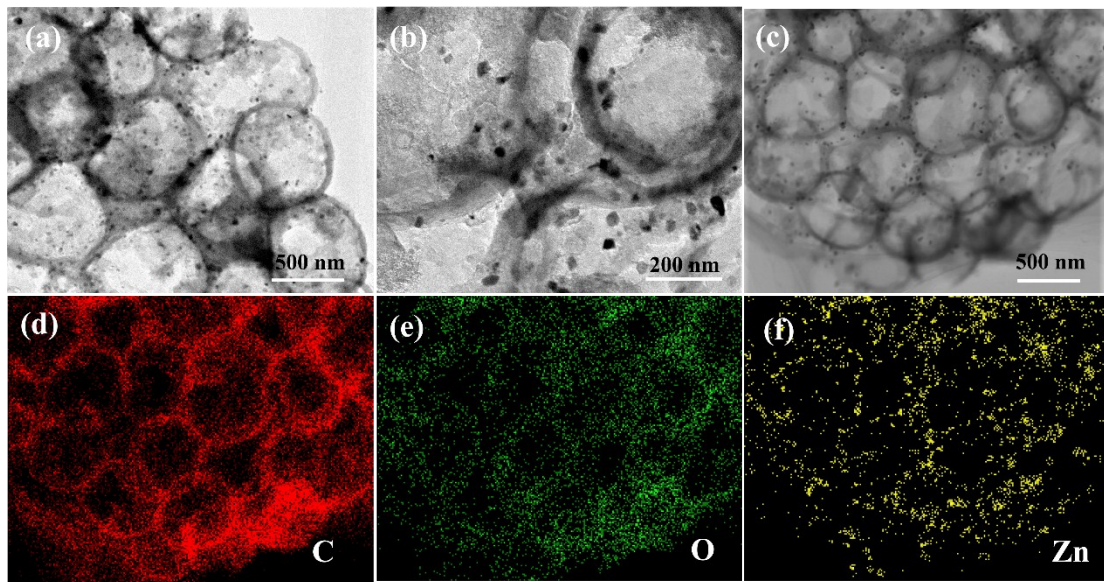


Fig. S10. Microstructure of 3D ZnO@PCCMs electrode stripping 2.0 mAh cm<sup>-2</sup> of lithium after 50 cycles with 2.0 mAh cm<sup>-2</sup> at 1.0 mA cm<sup>-2</sup>. (a-b) Typical TEM image of 3D ZnO@PCCMs electrode. (c-f) STEM image of 3D ZnO@PCCMs and the corresponding elemental mapping images of C, O and Zn.

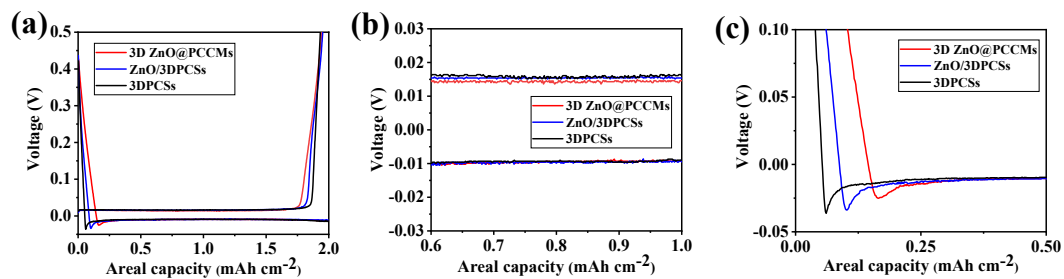


Fig. S11. Comparison of Voltage-Capacity profiles of Li plating/stripping on the 3D ZnO@PCCMs, 3DPCSs and ZnO/3DPCSs electrodes with a areal capacity of 2.0 mAh cm<sup>-2</sup> at a current density of 1.0 mA cm<sup>-2</sup>.

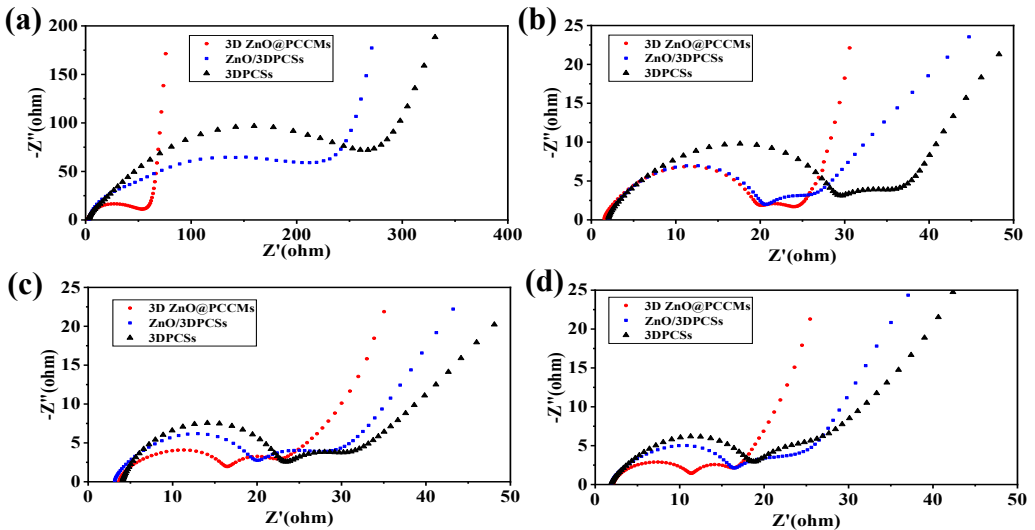


Fig. S12. Nyquist plots of the 3D ZnO@PCCMs, 3DPCSs and ZnO/3DPCSs electrodes (a) before cycling and after (b) 1 cycle, (c) 10 cycles and 30 cycles.

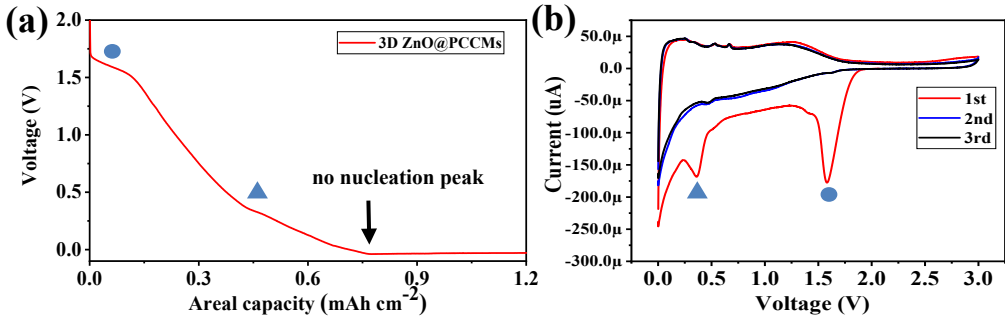


Fig. S13. (a) Voltage profiles of the 3D ZnO@PCCMs electrode during initial Li deposition at  $0.5 \text{ mA cm}^{-2}$ . (b) CV scans of the 3D ZnO@PCCMs electrode at a scan rate of  $0.5 \text{ mV s}^{-1}$ .

To understand the reactions that occurred during deposition, the electrochemical behavior of the half-cell based on the 3D ZnO@PCCMs (indicated with  $\text{Li||ZnO@PCCMs}$ , Li was used as anode and 3D ZnO@PCCMs as cathode) was investigated by cyclic voltammetry (CV), with the results presented in Fig. S6. During the first cathodic sweep, a wide peak appeared at 1.6 V and disappeared in the subsequent cycling, is attributed to the electrolyte decomposition and the formation of the SEI film on the electrode surface (Fig. S6b), well consistent with the corresponding voltage profile with a plateau at 1.6 V (Fig. S6a). Another peak at approximately 0.35 V in the first cathodic sweep could be associated with the conversion reaction where the ZnO is reduced by Li to form elemental Zn and  $\text{Li}_2\text{O}$  and the alloying reaction between Li and Zn (Fig. S6b). This can also be confirmed by the voltage profile, in which a small discharge plateau indicates that ZnO participated in the reaction during lithium deposition (Fig. S6a). In the anodic sweep, two small peaks in the range of 0.5~0.75V are responsible for the step-by-step de-alloying

---

reaction of Li-Zn alloy, and a wide peak at 1.25~1.5V is due to the reformation of ZnO. Based on Fig. S6a with the presence of a smooth voltage trace, it can be found that no nucleation peak upon further Li deposition was detected, indicating that the Li nucleation overpotential on ZnO is essentially zero.

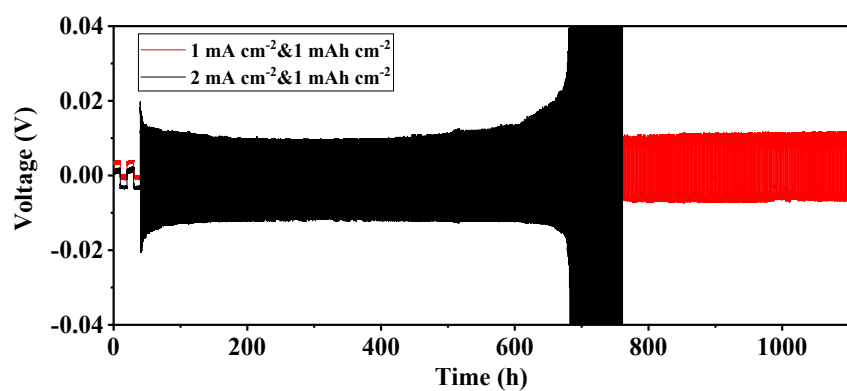


Fig. S14. Voltage profiles of metallic Li plating/stripping in the half cells of Li||Li-ZnO@PCCMs at  $1 \text{ mA cm}^{-2}$  for  $1 \text{ mAh cm}^{-2}$  and at  $2 \text{ mA cm}^{-2}$  for  $1 \text{ mAh cm}^{-2}$ .

Table S1. Comparison with Li metal anodes recently reported with high areal capacity working at high currents.

Reference	Current density (mA cm <sup>-2</sup> )	Areal capacity (mA h cm <sup>-2</sup> )	Columbic Efficiency (%)	Cycle number
<b>This work</b>	<b>1</b>	<b>2</b>	<b>99</b>	<b>250</b>
Ref.[S1]	0.5	1	98	300
Ref.[S2]	1	1	97	200
Ref.[S3]	1	1	97	150
Ref.[S4]	1	2	97	50
<b>This work</b>	<b>2</b>	<b>5</b>	<b>97</b>	<b>100</b>
Ref.[S4]	0.5	4	97	100
Ref.[S5]	2	4	99	90
Ref.[S6]	1	4.75	95	35
Ref.[S7]	1	5	97.5	100
<b>This work</b>	<b>5</b>	<b>5</b>	<b>96</b>	<b>80</b>
Ref.[S8]	5	5	90	40
Ref.[S9]	5	3	96	100

Table S2. Comparison of the rate performance of full batteries.

Reference	Rates	Reversible capacity (mAh g <sup>-1</sup> )	Cathode materials

<b>This work</b>	<b>2C</b>	<b>145</b>	<b>LiFePO<sub>4</sub></b>
Ref.[S10]	2C	135	LiFePO <sub>4</sub>
Ref.[S2]	2C	127	LiCoO <sub>2</sub>
Ref.[S9]	2C	115	LiFePO <sub>4</sub>
Ref. [S6]	2C	105	LiCoO <sub>2</sub>
Ref.[S11]	2C	80	LiFePO <sub>4</sub>
<b>This work</b>	<b>5C</b>	<b>120</b>	<b>LiFePO<sub>4</sub></b>
Ref.[S12]	4C	116	LiFePO <sub>4</sub>
Ref.[S10]	4C	115	LiFePO <sub>4</sub>
Ref.[S13]	5C	110	LiFePO <sub>4</sub>
Ref.[S2]	5C	104	LiCoO <sub>2</sub>
Ref.[S11]	5C	50	LiFePO <sub>4</sub>
Ref. [S6]	4C	10	LiCoO <sub>2</sub>

Table S3. Comparison of the cycling performance of full batteries.

Reference	Rates	Reversible capacity (mAh g <sup>-1</sup> )	Cycle number	Cathode materials
<b>This work</b>	<b>1 C</b>	<b>145</b>	<b>300</b>	<b>LiFePO<sub>4</sub></b>
Ref.[S10]	1 C	127.5	350	LiFePO <sub>4</sub>
Ref.[S2]	0.5 C	≈140	160	LiCoO <sub>2</sub>
Ref.[S5]	0.5 C	≈136	200	LiFePO <sub>4</sub>
Ref.[S9]	0.5 C	126	100	LiFePO <sub>4</sub>

---

Ref.[S6]	0.2 C	$\approx$ 100	40	LiCoO <sub>2</sub>
----------	-------	---------------	----	--------------------

## References

- S1 K. Yan, Z. Lu, H.-W. Lee, F. Xiong, P.-C. Hsu, Y. Li, J. Zhao, S. Chu and Y. Cui, *Nat. Energy*, 2016, **1**, 16010.
- S2 C. Jin, O. Sheng, J. Luo, H. Yuan, C. Fang, W. Zhang, H. Huang, Y. Gan, Y. Xia, C. Liang, J. Zhang and X. Tao, *Nano Energy*, 2017, **37**, 177.
- S3 G. Zheng, S. W. Lee, Z. Liang, H. W. Lee, K. Yan, H. Yao, H. Wang, W. Li, S. Chu and Y. Cui, *Nat. Nanotechnol.*, 2014, **9**, 618.
- S4 R. Zhang, S. Wen, N. Wang, K. Qin, E. Liu, C. Shi and N. Zhao, *Adv. Energy Mater.*, 2018, **8**, 1800914.
- S5 M. Hu, Y. Yuan, M. Guo, Y. Pan and D. Long, *J. Mater. Chem. A*, 2018, **6**, 14910.
- S6 H. Wang, D. Lin, J. Xie, Y. Liu, H. Chen, Y. Li, J. Xu, G. Zhou, Z. Zhang, A. Pei, Y. Zhu, K. Liu, K. Wang and Y. Cui, *Adv. Energy Mater.*, 2019, **9**, 1802720.
- S7 Z. Sun, S. Jin, H. Jin, Z. Du, Y. Zhu, A. Cao, H. Ji and L. J. Wan, *Adv. Mater.*, 2018, **30**, 1800884.
- S8 J. Xie, J. Ye, F. Pan, X. Sun, K. Ni, H. Yuan, X. Wang, N. Shu, C. Chen and Y. Zhu, *Adv. Mater.*, 2019, **31**, 1805654.
- S9 W. Deng, X. Zhou, Q. Fang and Z. Liu, *Adv. Energy Mater.*, 2018, **8**, 1703152.
- S10 H. Zhao, D. Lei, Y.-B. He, Y. Yuan, Q. Yun, B. Ni, W. Lv, B. Li, Q.-H. Yang, F. Kang and J. Lu, *Adv. Energy Mater.*, 2018, **8**, 1800266.
- S11 A. M. Hafez, Y. Jiao, J. Shi, Y. Ma, D. Cao, Y. Liu and H. Zhu, *Adv. Mater.*, 2018, **30**, 1802156.
- S12 B. Yu, T. Tao, S. Mateti, S. Lu and Y. Chen, *Adv. Funct. Mater.*, 2018, **28**, 1803023.
- S13 S. Liu, L. Deng, W. Guo, C. Zhang, X. Liu and J. Luo, *Adv. Mater.*, 2019, **31**, 1807585.